Starve a cold or feed a fever?

Identifying cellular metabolic changes following infection and exposure to SARS-CoV-2

Working title:

Metabolite profiling of SARS-CoV-2 infection

Emma Kate Loveday[a,c]*, Hope Welhaven[b], Ayten Ebru Erdogan[c], Kyle Hain[d], Connie B. Chang[a,c,e], Ronald K. June[f], Matthew P. Taylor[d]*

[a] Center for Biofilm Engineering, Montana State University, Bozeman MT 59717

[b] Chemistry and Biochemistry, Montana State University, Bozeman MT 59717

[c] Department of Chemical and Biological Engineering, Montana State University, Bozeman MT 59717

[d] Microbiology and Cell Biology, Montana State University, Bozeman MT 59717

[e] Department of Physiology and Biomedical Engineering, Mayo Clinic, Rochester, MN 55905

[f] Department of Mechanical & Industrial Engineering, Montana State University, Bozeman MT 59717

*Corresponding authors: mptaylor@montana.edu, emma.loveday@montana.edu

Abstract

Viral infections induce major shifts in cellular metabolism elicited by active viral replication and antiviral responses. For the virus, harnessing cellular metabolism and evading changes that limit replication are essential for productive viral replication. In contrast, the cellular response to infection disrupts metabolic pathways to prevent viral replication and promote an antiviral state in the host cell and neighboring bystander cells. This competition between the virus and cell results in measurable shifts in cellular metabolism that differ depending on the virus, cell type, and extracellular environment. The resulting metabolic shifts can be observed and analyzed using global metabolic profiling techniques to identify pathways that are critical for either viral replication or cellular defense. SARS-CoV-2 is a respiratory virus that can exhibit broad tissue tropism and diverse, yet inconsistent, symptomatology. While the factors that determine the presentation and severity of SARS-CoV-2 infection remain unclear, metabolic syndromes are associated with more severe manifestations of SARS-CoV-2 disease. Despite these observations a critical knowledge gap remains between cellular metabolic responses and SARS-CoV-2 infection. Using a well-established untargeted metabolomics analysis workflow, we compared SARS-CoV-2 infection of human lung carcinoma cells. We identified significant changes in metabolic pathways that correlate with either productive or non-productive viral infection. This information is critical for characterizing the factors that contribute to SARS-CoV-2 replication that could be targeted for therapeutic interventions to limit viral disease.

Introduction

As obligate intracellular parasites, viruses co-opt host cellular materials, machinery, and metabolism to facilitate viral replication (1,2). Metabolic changes in response to virus infection result in extensive alterations to cellular physiology and often mirror changes seen in cancer cells (2–7). Both RNA and DNA viruses reprogram different aspects of host metabolism including increased glycolysis, elevated pentose phosphate activity, amino acid generation and lipid synthesis (1). Viral hijacking of host metabolism and subversion of metabolic defenses can lead to increased viral replication and host damage, resulting in long-term health consequences, such as those seen in severe cases of COVID-19, following infection with the novel coronavirus, SARS-CoV-2. This is supported by analysis of SARS-CoV-2 positive patient serum that has shown acute and long-term changes in metabolites and further metabolic disorder (8–12).

To better understand what metabolic changes occur during SARS-CoV-2 infection and how this may relate to severe disease outcomes, we implemented global metabolomic profiling to analyze thousands of metabolites using LC-MS to detect disease-associated changes to the cellular environment (13,14). Metabolites serve as intermediates for cellular physiology and include hormones, oligonucleotides, peptides, and other molecular products of cellular biochemical reactions that represent the current physiological state of a cell (15). Global metabolomic profiling can therefore provide an unbiased view of metabolic shifts induced during and in response to viral infection (16,17).

To elucidate changes to cellular metabolism associated with SARS-CoV-2 viral replication and those changes associated with virus exposure we infected and profiled A549 cells, a human lung cell line. A549 cells are frequently used to evaluate viral infection for many respiratory viruses but are not intrinsically susceptible to SARS-CoV-2 infection, as they lack endogenous expression of the viral receptor, ACE2 (18–20). However, expression of human ACE2 protein on A549 (ACE2-A549) cells renders them fully susceptible to SARS-CoV-2 (21). By comparing A549 and ACE2-A549 cells inoculated with SARS-CoV-2 at an MOI of 10, we can identify, and separate metabolic

shifts induced by active viral replication from those induced by the host cells response to virus exposure.

Here, we describe distinct metabolic changes in to both ACE2-A549 and A549 cells triggered by SARS-CoV-2 exposure. Amino acid metabolism, glutathione, and urea cycle metabolic pathways were significantly altered in cells that support productive SARS-CoV-2 infection (ACE2-A549 cells). In contrast A549 cells that are not susceptible to infection but were exposed to a high inoculating dose of SARS-CoV-2 had significant changes in fatty acid anabolic and catabolic pathways as well as leukotriene metabolism. These results mirror the metabolic shifts found in serum from patients suffering from severe COVID-19 (10,11,17,22–27). Thus, our findings point to metabolite features associated with both active infection and exposure to virus. Understanding how cellular metabolism is reprogrammed following SARS-CoV-2 infection will allow identification of factors responsible for severe disease and aid in the development of antiviral therapies.

Materials and Methods

Cells and Viruses

E6-Vero, A549, ACE2-A549 cells. E6 Vero cells were obtained from ATCC (Manassas, VA) and grown in DMEM supplemented with 10% FBS, 1% pen-strep. A549 cells were the obtained from Chang Lab. ACE2-A549 cells were obtained from BEI Resources (NR-53821). A549 cells were propagated in Hams F-12 (Corning) media supplemented with 10% fetal bovine serum (HyClone) and 1X Penicillin/Streptomycin (Fisher Scientific). ACE2-A549 cells were supplemented with 100ug/mL Blasticidin (Gibco). SARS-CoV-2 strain WA01 was obtained from BEI Resources (NR-52281). Viral stocks were propagated and titered on E6 Vero cells in DMEM supplemented with 2% FBS and 1% pen-strep. Viral stocks were made by collecting media from infected cell cultures showing extensive cytopathic effect and centrifuged 1,000 RCF for 5 minutes to remove cellular debris. The clarified viral supernatant was then used for all experimental infection. For determination of viral infectivity by plaque assay, E6 Vero cells were cultured then incubated with viral inoculum at limiting dilutions. Following inoculation, cells were over-layered with 1% methylcellulose, DMEM supplemented with 2% FBS and 1% pen-strep and incubated for 3-4 days (28,29). Cells were then fixed and stained with 0.5% methylene blue/70% ethanol solution. Plaques were counted and the overall titer was calculated.

Immunofluorescence detection of infection

Prior to infection, cells were seeded at 2 x 10^4 per well of an eight-chamber coverslip (Labtek Cat. No. 155411, Nunc International, Rochester, NY). At indicated times post infection, cells were then fixed with 4% paraformaldehyde in PBS for 30 minutes, washed thoroughly with PBS, and blocked in 2% bovine serum albumin (BSA) prior to antibody incubations. Primary and secondary antibodies were diluted in a PBS supplemented with 0.5% saponin, 0.125% BSA as described (30), and incubated for one hour at room temperature. Primary mouse anti-nucleocapsid (Thermofisher) was diluted 1:500, followed by goat anti-mouse IgG labeled with Dylight 550 (Thermofisher) at 1:500. DNA was counterstained with Hoescht 3342 at 1:5000 dilution. Actin filaments stained with phalloidin-488 (Thermofisher) at 1:500. Stained cells were imaged on a

Nikon Ti-Eclipse inverted epifluorescent microscope (Nikon Instruments, Melville, NY) equipped with an iXon 896 EM-CCD (Andor Technology Ltd., Belfast, Northern Ireland) camera. Fluorescence detection used a SpectraX LED light engine (Lumencor, Beaverton, OR) with paired excitation filters, dichroic mirrors, and emission filters (Prior Scientific, Rockland, MA). Images were acquired with either Plan Fluor 20 phase contrast (Ph) air objective or CFI Plan Apochromat Lambda 60x Oil immersion objective. All imaging experiments were performed a minimum of two times.

Metabolite Extractions

After SARS-CoV-2 inoculation for one hour, cells were washed with PBS then fed with fresh media. Cells were harvested at 0-, 6-, and 16-hours post-inoculum removal. At each collection, cells were washed with PBS, suspended with trypsin-EDTA for 5 minutes, collected and centrifuged for 5 minutes. Trypsin-EDTA was removed, and cell pellets were washed with an equi-volume of PBS before repeated centrifugation. PBS was removed and cells were resuspended in 100% methanol. Samples were vortexed in 10 x 1 sec bursts before being placed in -80°C freezer. Vortexing and freezing was repeated 3 times to maximize macromolecule precipitation. Subsequently, methanol extracts were subjected to centrifugation at 8,000 rcf for 10 minutes to pellet cell debris and precipitate proteins. The supernatant containing the metabolites was transferred to a separate tube and dried by vacuum concentration to remove solvents. Dried metabolites were resuspended in 100 μL mass spectrometry grade 50:50 (v/v) water: acetonitrile solution immediately prior to high performance liquid chromatography-mass spectrometry (HPLC-MS) analysis.

Untargeted Metabolomic Analysis

Extracted metabolites were analyzed using HPLC-MS (Agilent 6538 Q-TOF mass spectrometer) in positive mode (resolution: ~20ppm, accuracy: ~5ppm, possible ionization adducts: H^+, Na^+) using a Cogent Diamond Hydride HILIC column (150 x 2.1 mm). LC-MS data, consisting of mass-to-charge (m/z) values and their peak intensities, were processed and exported using MSConvert and XCMS **(Table S1)**. All data was log transformed and autoscaled prior to analysis using MetaboAnalyst (31–33). Statistical analyses performed included hierarchical cluster analysis (HCA), principal component

158 analysis (PCA), partial least-squares discriminant analysis (PLS-DA), variable
159 importance in projection (VIP) scores, volcano plot, fold change, and heatmap analysis.
160 Pathway analysis was performed to map differentially expressed metabolite features to
161 biological pathways using the Functional Analysis function in MetaboAnalyst (pathway
162 library: KEGG, mass tolerance: 5 ppm, positive mode) (31,32). Pathway significance
163 was determined using FDR-corrected significance levels of 0.05.

164

165

Results

Differing susceptibility and productivity of A549 cells lines for SARS-CoV-2

To study metabolic shifts during SARS-CoV-2 infection, we analyzed A549 cells, a human lung carcinoma cell line. A549 cells are not susceptible to SARS-CoV2 infection and must be modified to express human ACE2 to allow for entry and replication (18–21). Therefore, we analyzed infection of A549 cells with (ACE2-A549) and without (A549) human ACE2 expression at 0, 6 and 16 hours post infection (hpi) to explore how differences in susceptibility and relative timing of viral replication impact cellular metabolism. The differences in infection enabled us to explore metabolic changes in cells that can support robust productive virus infection and in cells that do not allow viral entry. Our analysis focuses on three critical timepoints: 0 hours post infection (hpi), or immediately after inoculum removal, 6 hpi, a timepoint suggested to be prior to the onset of progeny virus production, and 16 hpi, when productive viral replication should be close to its peak (34).

The extent of viral infection and replication was analyzed using indirect immunofluorescent detection of the SARS-CoV-2 nucleocapsid (N) protein **(Figure 1A)**. ACE2-A549 cells displayed extensive N protein expression at both 6 and 16 hpi. In contrast, unmodified A549 cells displayed no N protein staining, indicating a complete lack of infection and replication following SARS-CoV-2 inoculation. An important element to analyzing metabolic profiles is the relative “health” of the cell, especially at later time points in the viral lifecycle. To evaluate whether 16 hpi exhibits extensive cell deterioration, we analyzed the distribution of actin filaments in infected cells. Cells were counterstained with both SARS-CoV-2 nucleocapsid (N) protein and phalloidin to image for the presence of actin filament assemblies during infection **(Figure 1B)**. We observed a distribution of cellular morphologies, but many cells retain actin filament assemblies and adhesions to the cell surface similar to uninfected cells. The distribution of cellular morphology and actin staining suggests that the cells are not undergoing extensive cytopathic effect or cell death by 16 hpi.

To understand how the selected timepoints correlate with viral replication, we analyzed viral titers from supernatant with (total) and without (extracellular) cellular

fractions, **(Figure 1C)**. We compared the detection of plaque forming units (PFU) from ACE2-A549 and A549 cells at all three timepoints. In the ACE2-A549 cells, viral titer does not increase until 16 hours post inoculation in both the total and extracellular samples. A decrease at 6 hpi in the extracellular samples reflects the uptake of viral inoculum. The subsequent increase in titer at 16 hpi correlates with the release of virus. For A549 cells there was no increase in viral titer in either the total or extracellular samples beyond what is detected after inoculation of cells. These observations are consistent with the reported lack of susceptibility and permissiveness of A549 cells to SARS-CoV-2 (19,20).

Experimental design to assess metabolic differences following SARS-CoV-2 infection

Global metabolomic profiling was performed in cells infected with or exposed to SARS-CoV-2. In our experimental approach, ACE2-A549 and A549 cells were inoculated at an MOI of 10 with SARS-CoV-2 to ensure that every cell was sufficiently exposed to infectious virions. The cells were collected and processed at 0, 6, and 16 hpi, to analyze temporal changes in the metabolic landscape over the course of the viral lifecycle **(Figure 2A)**. Metabolites were extracted and processed for LC-MS metabolite detection **(Figure 2B)**. Samples were analyzed via LC-MS to identify molecules smaller than ~1000 Da, which can include hormones, oligonucleotides, peptides, and other molecular products of cellular biochemical reactions (31,32). A total of 1085 metabolites were detected across all samples and were included in all analyses. Data analyses were performed using MetaboAnalyst allowing for quantification of untargeted metabolites and identification of changes in the metabolomic phenotypes at each of the different time points **(Figure 2C)** (31–33)**.**

Metabolic profiling of ACE2-A549 cells during SARS-CoV-2 infection

We began by analyzing metabolic changes in ACE2-A549 cells that support productive SARS-CoV-2 infection. Changes in the global metabolomic profiles of infected ACE2-A549 cells were determined using unsupervised PCA and supervised PLS-DA (**Figure 3A & B**). From these analyses, the variance between each time point was greater than the variance between replicates within each group. We observed that

the first 2 PLS-DA components represented 42% of the overall variance, further demonstrating that the three time points are distinct from each other. This is much greater than the expected 0.03% variance that would be expected from a uniformly random distribution of metabolites. Taken together, our data suggests that greater metabolomic changes occur over time although some overlap between samples is observed. Both analyses confirm that clear, non-random, differences exist between productively infected ACE2-A549 cells harvested at different each time points.

To further examine metabolomic patterns that significantly change during SARS-CoV-2 infection in ACE2-A549 cells, we performed ANOVA to assess changes in metabolomic between cells harvested at 0, 6, and 16 hpi. From this analysis, 152 metabolite features with an FDR-corrected p-value < 0.05 were differentially regulated between timepoint groups. Heatmap analysis of these ANOVA metabolite features revealed temporal changes in metabolite phenotypes from 0 to 16 hpi **(Figure 3C)**. The variance between samples can also be observed when each metabolite feature is plotted for the individual samples **(SI Figure 1)**. Clustering analysis of similarly altered metabolite feature produces 4 main classes: reduced at 16 hpi (class 1), increased at 16 hpi (class 2), reduced at 6 hpi (class 3), and increased at 6 hpi (class 4). The majority of altered metabolite features, belonging to class 1, had the highest abundance at 0 hpi and progressively decreased from 6 to 16 hpi, suggesting a trajectory of depletion during the course of SARS-CoV-2 replication. In contrast, class 2 metabolite features increased in abundance from 0 to 16 hpi. For classes 3 and 4, metabolite features with detected changes at 6 hpi often returned to baseline abundance by 16 hpi.

To derive additional biological relevance, the 152 metabolite features distinguished by ANOVA were then manually searched by m/z value in METLIN to make putative metabolite identifications (35). Identified putative metabolites were found in the four main classes **(Figure 3C).** Select metabolites are presented to highlight some of the metabolic changes detected during infection **(Figure 4).** Each boxplot depicts the normalized fold-change of the putative metabolite description for each class with average values represented as yellow diamonds and individual replicates within each time point represented as black spots. These metabolite features may be

associated with some flux or alteration in utilization of intermediates in metabolic pathways.

Distinct metabolic phenotypes of A549 cells during SARS-CoV-2 infection

We next sought to separate metabolic changes identified during productive infection from changes that may result from responses due to virus exposure. To accomplish this, we analyzed A549 cells, which do not express ACE2 and are refractory to infection at 0, 6 and 16 hpi after exposure to SARS-CoV-2 inoculum (19,20). As before, we evaluated metabolomic phenotypes using PCA and PLS-DA and observed larger ellipses that somewhat overlap. PLS-DA components 1 and 2 represented 43.2% of the overall variance in the dataset. Similar to the ACE2-A549 cells, these findings suggest that metabolomic differences between A549 cells harvested at different timepoints exist, despite no detectable infection or viral replication. **(Figure 5A and B)**. From the inoculated A549 cells, we identified 377 metabolite features that had an ANOVA FDR-corrected p-value < 0.05. To further visualize metabolic dysregulation across 0, 6, and 16 hpi, heatmap analysis was performed **(Figure 5C)**. The distribution and consistency of detected metabolite features across the replicate samples can be seen in the expanded heatmap **(SI figure 2)**. Unlike with ACE2-A549 cells, the majority of metabolic changes are increasing quantities of metabolite features that peak at 6 hpi and remain elevated through 16 hpi **(Figure 5C)**. The second prominent class of metabolite features exhibits a transient increase in detection at 6 hpi, followed by reduced detection at or near levels seen at 0 hpi. The remaining significantly changed metabolite features vary with peak detection seen either at 0 or 16 hpi. Overall, the majority of changes in these cells likely represent changes in response to the inoculum that decrease by the later time points after inoculation.

Comparison of metabolites between ACE2 and A549 cells.

We sought to further understand the differing metabolic responses between A549 cells exposed to SARS-CoV-2 and ACE2-A549 cells infected with SARS-CoV-2. Statistically significant features distinguished by ANOVA analyses for both comparisons were investigated to identify metabolite features that were either shared or unique between the two cell types. Of the 152 significant metabolite features from ACE2-A549

cells and 377 significant metabolite features from A549 cells, only 47 were significantly changed following SARS-CoV-2 exposure in both cell types **(Figure 6A)**. In addition, pathway analysis of metabolite features that are dysregulated during SARS-CoV-2 replication was performed **(Figure 6B)**.

In total, 13 metabolic pathways were altered in ACE2-A549 cells with productive SARS-CoV-2 replication. A majority, 10 pathways, were involved in amino acid metabolism including alanine, aspartate, cysteine, glutamate, glycine, histidine, lysine, methionine, and threonine **(Table 1)**. Additional metabolic pathways detected included glycerophospholipid metabolism, C5-branched dibasic acid metabolism, and ascorbate metabolism. Identifying if these altered pathways are caused by productive viral replication cannot be assessed from this data alone. We compared pathway changes in cells that cannot be productively infected by SARS-CoV-2. Performing pathway analysis on the 377 metabolite features distinguished by ANOVA from the A549 cells inoculated with SARS-CoV-2 identified 8 distinct pathways. Curiously, none of these pathways overlap with those identified in from ACE2-A549 analysis **(Figure 6B)**. The 8 pathways unique to A549 cells mapped exclusively to lipid metabolism and included: fatty acid oxidation, activation, and metabolism; di-unsaturated fatty acid beta-oxidation, de novo fatty acid biosynthesis, omega-3 fatty acid metabolism, and carnitine shuttle **(Table 2)**. Interestingly, metabolite features associated with immunomodulatory leukotrienes were also detected. Overall, these extensive changes to lipids, specifically fatty acids, suggest a change not only towards an inflammatory state, but also a shift in energy source by the cells following exposure to a non-productive infection.

Taken together, changes in metabolism between two cell lines over a 16-hour period of exposure to SARS-CoV-2 demonstrate metabolomic differences in a range of individual metabolites and pathways. Specifically, amino acid related-pathways were dysregulated in ACE2-A540 while lipid-related pathways were dysregulated in A549 cells exposed to SARS-COV2 **(Figure 6C)**.

Discussion

In this study, we sought to understand the nature of cellular metabolic shifts in response to SARS-CoV-2 infection. To distinguish changes associated with viral replication from exposure to infectious virus, we compared ACE2-expressing A549 cells that are susceptible and support productive viral replication with A549 cells that are not susceptible to infection. We chose time points that represent early, intermediate, and late stages of viral replication to evaluate the temporal changes in metabolites following inoculation. Our metabolic pathway analysis found 152 and 377 significantly changed metabolites in ACE2-A549 and A549 cells, respectively. Surprisingly, there was limited overlap in altered metabolites or altered metabolic pathways between cells undergoing productive infection and those exposed to infectious virus. Critically, we identified alterations in pathways that are potentially involved in either productive viral infection or in cellular anti-viral responses to SARS-CoV-2.

Consequences of productive viral infection

The initial focus of our analysis was the changes to cellular metabolism induced by active viral replication. The ACE2-A549 cells are a widely used model that we observed to be both susceptible to SARS-CoV-2 infection and permissive for productive viral replication (34). We analyzed metabolic shifts immediately after virion entry (0 hpi), a mid-point of viral replication prior to virion production (6 hpi), and a late timepoint when new virions are being released from infected cells (16 hpi) (17). Overall, we identified four different classes of metabolites based on the relative increase or decrease in detection between each time point. We used these changes to identify pathways that were altered by active SARS-CoV-2 replication. Most notably, we observed that the majority of altered metabolic pathways were associated with amino acid metabolism.

Within the identified pathways, we identified L-Glutamic Acid as a major putative metabolite that was significantly reduced from 0 to 16 hpi. A previous study demonstrated that SARS-CoV-2 infection rewires carbon entry into the TCA cycle (17). Mullen et al. showed that oxidative metabolism of glutamine through the TCA cycle was reduced during SARS-CoV-2 infection in favor of pyruvate utilization via pyruvate

carboxylase (35,36). This shift increased levels of oxaloacetate and also maintain synthesis of aspartate, which is used to synthesize pyrimidine nucleotides (36,37). Interestingly, both glutamate and aspartate metabolic pathways were considered significant in our analysis of SARS-CoV-2 infected ACE2-A549 cells.

In addition to changes to L-glutamic acid and aspartate, the metabolic shifts observed in SARS-CoV-2 infected ACE2-A549 cells reflect similar changes observed in COVID-19 positive patient serum samples (10,23,27,38–43). It is notable that our cell culture model identified similar metabolic pathways being disrupted during SARS-CoV-2 infection, even at 6 hpi. This indicates that metabolic screening of different laboratory-based model systems may be able to accurately generate data on potential biomarkers for SARS-CoV-2 and potentially other infectious diseases.

Metabolites responding to viral inoculation

While metabolic changes due to active viral replication are important, not all cells within a tissue or organ system are equally susceptible to virus infection. Thus, we hypothesized that uninfected cells that do not support SARS-CoV-2 infection can respond to virus exposure with altered metabolism leading to further metabolic dysfunction. To test this hypothesis, we analyzed the metabolic profile of A549 cells that do not support viral entry following exposure to the same infectious virus inoculum as the ACE2-A549 cells. Our data confirmed that lack of ACE2 expression in A549 cells resulted in a complete lack of infection and replication following SARS-CoV-2 inoculation. While we have no evidence of viral replication in A549 cells, the resulting changes in the metabolic profile of these cells indicates that they are responding to the virus inoculum. Specifically, fatty acid catabolic (β-oxidation) and anabolic (de novo fatty acid synthesis) pathways were significantly altered following A549 cell exposure to infectious virus. Lipid dysregulation has been a hallmark of COVID-19 pathology in patients and a hallmark of disease severity and progression (41,44,45). Both pathways converge on acetyl-CoA, a critical molecule in the breakdown of fatty acids and the synthesis of other lipid types, such as cholesterol, which can be transformed into other steroids with pro and anti-inflammatory mechanisms (46,47). This is further supported by the significant number of identified metabolites associated with leukotriene and

omega-3 fatty acid metabolism within the A549 cells. Increased leukotriene production is connected to COVID-19 through transcriptional and metabolic studies from patient serum and infected monocytes (48–50). Another significant metabolite in our profile of the A549 cells was palmitoyl-CoA, a major component in the synthesis of ceramide and sphingolipids (51). Previous studies of COVID-19 patient serum samples found distinct increases in sphingosine and ceramides (52,53). These increases were distinct between patients with mild disease and those in intensive care (53). The data suggests that uninfected cells respond to SARS-CoV-2, altering metabolic profiles and possibly increasing the production of pro- or anti-inflammatory biomolecules and enzyme cofactors (3,4,54). Thus, even uninfected cells may be contributing to the overall pathology observed in COVID-19 patients.

Conclusion

Cellular models for SARS-CoV-2 infection are incredibly important for the initial testing of interventions that directly target viral replication. Through our metabolomic profiling, we identified metabolites and metabolic profiles that are associated with both active viral infection and exposure to infectious virus. Our analysis identified a range of metabolites and metabolic pathways altered by productive viral replication, but understanding if these metabolites are promoting viral replication will require further analysis. While cellular metabolism is often thought to be manipulated by the virus for its own ends, it is also connected to antiviral responses (1–3). Cells can produce antiviral metabolites or inhibit metabolic pathways to hinder viral replication (3). As with productive replication, further experiments that either promote shifts in leukotrienes or other inflammatory molecules will need to be performed to characterize their effects on SARS-CoV-2 infection. It is also possible that the identified metabolite profiles can be developed as biomarkers of infection that could be used for surveillance testing or as a predictive tool for risk evaluation of severe disease. The similarities of our results to metabolic shifts observed in patients suggest a potential platform for methodological development. Discriminatory metabolites defining infection can be correlated to patient metabolic profiles to facilitate our understanding of SARS-CoV-2 induced pathologies. Through both the immediate findings and the development of more complex models, we hope to increase our understanding of how SARS-CoV-2 replication and spread correlates to

disease. Through that understanding, we can then find better therapeutics to limit morbidity and mortality from COVID-19.

Acknowledgments

The authors acknowledge funding from NSF (CMMI 1554708), NIH (NIAMS R01AR073964 and R01AR081489 and NIAID 1R56AI156137-01), and a Montana State University VPREDGE COVID Research Award. The following reagent was obtained through BEI Resources, NIAID, NIH: Human Lung Carcinoma Cells (A549) Expressing Human Angiotensin-Converting Enzyme 2, NR-53821. The following reagent was deposited by the Centers for Disease Control and Prevention and obtained through BEI Resources, NIAID, NIH: SARS-Related Coronavirus 2, Isolate USA-WA1/2020, NR-52281. Funding for the Montana State Mass Spectrometry Facility used in this publication was made possible in part by the MJ Murdock Charitable Trust, the National Institute of General Medical Sciences of the National Institutes of Health under Award Numbers P20GM103474 and S10OD28650, and the MSU Office of Research and Economic Development. The content is solely the responsibility of the authors and does not necessarily represent the official views of the National Institutes of Health.

References

1. Thaker SK, Ch'ng J, Christofk HR. Viral hijacking of cellular metabolism. BMC Biol. 2019 Jul 18;17(1):59.

2. Sanchez EL, Lagunoff M. Viral activation of cellular metabolism. Virology. 2015 May;479–480:609–18.

3. Palmer CS. Innate metabolic responses against viral infections. Nat Metab. 2022 Oct;4(10):1245–59.

4. Sánchez-García FJ, Pérez-Hernández CA, Rodríguez-Murillo M, Moreno-Altamirano MMB. The Role of Tricarboxylic Acid Cycle Metabolites in Viral Infections. Front Cell Infect Microbiol. 2021 Sep 14;11:725043.

5. Thai M, Thaker SK, Feng J, Du Y, Hu H, Ting Wu T, et al. MYC-induced reprogramming of glutamine catabolism supports optimal virus replication. Nat Commun. 2015 Nov 12;6:8873.

436 6. Brenner C. Viral infection as an NAD+ battlefield. Nat Metab. 2022 Jan;4(1):2–3.

437 7. Proal AD, VanElzakker MB. Pathogens Hijack Host Cell Metabolism: Intracellular
438 Infection as a Driver of the Warburg Effect in Cancer and Other Chronic
439 Inflammatory Conditions. Immunometabolism. 2021 Jan;3(1):e210003.

440 8. Wu Q, Zhou L, Sun X, Yan Z, Hu C, Wu J, et al. Altered Lipid Metabolism in
441 Recovered SARS Patients Twelve Years after Infection. Sci Rep. 2017 Aug
442 22;7(1):9110.

443 9. Lodge S, Nitschke P, Kimhofer T, Coudert JD, Begum S, Bong S-H, et al. NMR
444 Spectroscopic Windows on the Systemic Effects of SARS-CoV-2 Infection on
445 Plasma Lipoproteins and Metabolites in Relation to Circulating Cytokines. J
446 Proteome Res. 2021 Feb 5;20(2):1382–96.

447 10. Ansone L, Briviba M, Silamikelis I, Terentjeva A, Perkons I, Birzniece L, et al.
448 Amino Acid Metabolism is Significantly Altered at the Time of Admission in Hospital
449 for Severe COVID-19 Patients: Findings from Longitudinal Targeted Metabolomics
450 Analysis. Microbiol Spectr. 2021 Dec 22;9(3):e0033821.

451 11. Rees CA, Rostad CA, Mantus G, Anderson EJ, Chahroudi A, Jaggi P, et al. Altered
452 amino acid profile in patients with SARS-CoV-2 infection. Proc Natl Acad Sci U S A
453 [Internet]. 2021 Jun 22;118(25). Available from:
454 http://dx.doi.org/10.1073/pnas.2101708118

455 12. Loo RL, Lodge S, Kimhofer T, Bong S-H, Begum S, Whiley L, et al. Quantitative in-
456 vitro diagnostic NMR spectroscopy for lipoprotein and metabolite measurements in
457 plasma and serum: Recommendations for analytical artifact minimization with
458 special reference to COVID-19/SARS-CoV-2 samples. J Proteome Res. 2020 Nov
459 6;19(11):4428–41.

460 13. Carlson AK, Rawle RA, Adams E, Greenwood MC, Bothner B, June RK.
461 Application of global metabolomic profiling of synovial fluid for osteoarthritis
462 biomarkers. Biochem Biophys Res Commun. 2018 May 5;499(2):182–8.

463 14. Carlson AK, Rawle RA, Wallace CW, Brooks EG, Adams E, Greenwood MC, et al.
464 Characterization of synovial fluid metabolomic phenotypes of cartilage
465 morphological changes associated with osteoarthritis. Osteoarthritis Cartilage. 2019
466 Aug;27(8):1174–84.

467 15. Giera M, Yanes O, Siuzdak G. Metabolite discovery: Biochemistry's scientific
468 driver. Cell Metab. 2022 Jan 4;34(1):21–34.

469 16. Zhang Y, Guo R, Kim SH, Shah H, Zhang S, Liang JH, et al. SARS-CoV-2 hijacks
470 folate and one-carbon metabolism for viral replication. Nat Commun. 2021 Mar
471 15;12(1):1676.

17. Mullen PJ, Garcia G Jr, Purkayastha A, Matulionis N, Schmid EW, Momcilovic M, et al. SARS-CoV-2 infection rewires host cell metabolism and is potentially susceptible to mTORC1 inhibition. Nat Commun. 2021 Mar 25;12(1):1876.

18. Tian X, Zhang K, Min J, Chen C, Cao Y, Ding C, et al. Metabolomic Analysis of Influenza A Virus A/WSN/1933 (H1N1) Infected A549 Cells during First Cycle of Viral Replication. Viruses. 2019 Oct 31;11(11):1007.

19. Blanco-Melo D, Nilsson-Payant BE, Liu W-C, Uhl S, Hoagland D, Møller R, et al. Imbalanced Host Response to SARS-CoV-2 Drives Development of COVID-19. Cell. 2020 May 13;181(5):1036-1045.e9.

20. Hoffmann M, Kleine-Weber H, Schroeder S, Krüger N, Herrler T, Erichsen S, et al. SARS-CoV-2 Cell Entry Depends on ACE2 and TMPRSS2 and Is Blocked by a Clinically Proven Protease Inhibitor. Cell. 2020 Apr 16;181(2):271-280.e8.

21. Mossel EC, Huang C, Narayanan K, Makino S, Tesh RB, Peters CJ. Exogenous ACE2 Expression Allows Refractory Cell Lines To Support Severe Acute Respiratory Syndrome Coronavirus Replication. J Virol. 2005 Mar;79(6):3846–50.

22. Sohrabi Y, Reinecke H, Godfrey R. Altered Cholesterol and Lipid Synthesis Mediates Hyperinflammation in COVID-19. Trends Endocrinol Metab. 2021 Mar;32(3):132–4.

23. Páez-Franco JC, Torres-Ruiz J, Sosa-Hernández VA, Cervantes-Díaz R, Romero-Ramírez S, Pérez-Fragoso A, et al. Metabolomics analysis reveals a modified amino acid metabolism that correlates with altered oxygen homeostasis in COVID-19 patients. Sci Rep. 2021 Mar 18;11(1):6350.

24. Matsuyama T, Yoshinaga SK, Shibue K, Mak TW. Comorbidity-associated glutamine deficiency is a predisposition to severe COVID-19. Cell Death Differ. 2021 Dec;28(12):3199–213.

25. Thomas T, Stefanoni D, Reisz JA, Nemkov T, Bertolone L, Francis RO, et al. COVID-19 infection results in alterations of the kynurenine pathway and fatty acid metabolism that correlate with IL-6 levels and renal status. medRxiv [Internet]. 2020 May 16; Available from: http://dx.doi.org/10.1101/2020.05.14.20102491

26. da Silva Fidalgo TK, Freitas-Fernandes LB, Marques BBF, de Araújo CS, da Silva BJ, Guimarães TC, et al. Salivary Metabolomic Analysis Reveals Amino Acid Metabolism Shift in SARS-CoV-2 Virus Activity and Post-Infection Condition. Metabolites [Internet]. 2023 Feb 11;13(2). Available from: http://dx.doi.org/10.3390/metabo13020263

27. Blasco H, Bessy C, Plantier L, Lefevre A, Piver E, Bernard L, et al. The specific metabolome profiling of patients infected by SARS-COV-2 supports the key role of tryptophan-nicotinamide pathway and cytosine metabolism. Sci Rep. 2020 Oct 8;10(1):16824.

28. Jureka AS, Silvas JA, Basler CF. Propagation, Inactivation, and Safety Testing of SARS-CoV-2. Viruses [Internet]. 2020 Jun 6;12(6). Available from: http://dx.doi.org/10.3390/v12060622

29. Hotchin JE. Use of methyl cellulose gel as a substitute for agar in tissue-culture overlays. Nature. 1955 Feb 19;175(4451):352.

30. Jackson WT, Giddings TH Jr, Taylor MP, Mulinyawe S, Rabinovitch M, Kopito RR, et al. Subversion of cellular autophagosomal machinery by RNA viruses. PLoS Biol. 2005 May;3(5):e156.

31. Xia J, Wishart DS. Using MetaboAnalyst 3.0 for Comprehensive Metabolomics Data Analysis. Curr Protoc Bioinformatics. 2016 Sep 7;55:14.10.1-14.10.91.

32. Pang Z, Zhou G, Ewald J, Chang L, Hacariz O, Basu N, et al. Using MetaboAnalyst 5.0 for LC–HRMS spectra processing, multi-omics integration and covariate adjustment of global metabolomics data. Nat Protoc. 2022 Jun 17;17(8):1735–61.

33. Chong J, Soufan O, Li C, Caraus I, Li S, Bourque G, et al. MetaboAnalyst 4.0: towards more transparent and integrative metabolomics analysis. Nucleic Acids Res. 2018 Jul 2;46(W1):W486–94.

34. Ogando NS, Dalebout TJ, Zevenhoven-Dobbe JC, Limpens RWAL, van der Meer Y, Caly L, et al. SARS-coronavirus-2 replication in Vero E6 cells: replication kinetics, rapid adaptation and cytopathology. J Gen Virol. 2020 Sep;101(9):925–40.

35. Guijas C, Montenegro-Burke JR, Domingo-Almenara X, Palermo A, Warth B, Hermann G, et al. METLIN: A technology platform for identifying knowns and unknowns. Anal Chem. 2018 Mar 6;90(5):3156–64.

36. Birsoy K, Wang T, Chen WW, Freinkman E, Abu-Remaileh M, Sabatini DM. An Essential Role of the Mitochondrial Electron Transport Chain in Cell Proliferation Is to Enable Aspartate Synthesis. Cell. 2015 Jul 30;162(3):540–51.

37. Sullivan LB, Gui DY, Hosios AM, Bush LN, Freinkman E, Vander Heiden MG. Supporting Aspartate Biosynthesis Is an Essential Function of Respiration in Proliferating Cells. Cell. 2015 Jul 30;162(3):552–63.

38. Lawler NG, Gray N, Kimhofer T, Boughton B, Gay M, Yang R, et al. Systemic Perturbations in Amine and Kynurenine Metabolism Associated with Acute SARS-CoV-2 Infection and Inflammatory Cytokine Responses. J Proteome Res. 2021 May 7;20(5):2796–811.

39. Caterino M, Costanzo M, Fedele R, Cevenini A, Gelzo M, Di Minno A, et al. The Serum Metabolome of Moderate and Severe COVID-19 Patients Reflects Possible Liver Alterations Involving Carbon and Nitrogen Metabolism. Int J Mol Sci [Internet]. 2021 Sep 2;22(17). Available from: http://dx.doi.org/10.3390/ijms22179548

40. Ayres JS. A metabolic handbook for the COVID-19 pandemic. Nat Metab. 2020 Jul;2(7):572–85.

41. Wu D, Shu T, Yang X, Song J-X, Zhang M, Yao C, et al. Plasma metabolomic and lipidomic alterations associated with COVID-19. Natl Sci Rev. 2020 Jul;7(7):1157–68.

42. Shi D, Yan R, Lv L, Jiang H, Lu Y, Sheng J, et al. The serum metabolome of COVID-19 patients is distinctive and predictive. Metabolism. 2021 May;118:154739.

43. Li X, Liu Y, Xu G, Xie Y, Wang X, Wu J, et al. Plasma metabolomic characterization of SARS-CoV-2 Omicron infection. Cell Death Dis. 2023 Apr 19;14(4):276.

44. Bruzzone C, Bizkarguenaga M, Gil-Redondo R, Diercks T, Arana E, García de Vicuña A, et al. SARS-CoV-2 Infection Dysregulates the Metabolomic and Lipidomic Profiles of Serum. iScience. 2020 Oct 23;23(10):101645.

45. Gardinassi LG, Servian C do P, Lima G da S, Dos Anjos DCC, Gomes Junior AR, Guilarde AO, et al. Integrated Metabolic and Inflammatory Signatures Associated with Severity of, Fatality of, and Recovery from COVID-19. Microbiol Spectr. 2023 Feb 28;11(2):e0219422.

46. Wang Y, Yang H, Geerts C, Furtos A, Waters P, Cyr D, et al. The multiple facets of acetyl-CoA metabolism: Energetics, biosynthesis, regulation, acylation and inborn errors. Mol Genet Metab. 2023 Jan;138(1):106966.

47. Cerqueira NMFSA, Oliveira EF, Gesto DS, Santos-Martins D, Moreira C, Moorthy HN, et al. Cholesterol Biosynthesis: A Mechanistic Overview. Biochemistry. 2016 Oct 4;55(39):5483–506.

48. Citron F, Perelli L, Deem AK, Genovese G, Viale A. Leukotrienes, a potential target for Covid-19. Prostaglandins Leukot Essent Fatty Acids. 2020 Oct;161:102174.

49. Archambault A-S, Zaid Y, Rakotoarivelo V, Turcotte C, Doré É, Dubuc I, et al. High levels of eicosanoids and docosanoids in the lungs of intubated COVID-19 patients. FASEB J. 2021 Jun;35(6):e21666.

50. Pérez MM, Pimentel VE, Fuzo CA, da Silva-Neto PV, Toro DM, Fraga-Silva TFC, et al. Acetylcholine, Fatty Acids, and Lipid Mediators Are Linked to COVID-19 Severity. J Immunol. 2022 Jul 15;209(2):250–61.

51. Hannun YA, Obeid LM. Sphingolipids and their metabolism in physiology and disease. Nat Rev Mol Cell Biol. 2018 Mar;19(3):175–91.

52. Vitner EB, Avraham R, Politi B, Melamed S, Israely T. Elevation in sphingolipid upon SARS-CoV-2 infection: possible implications for COVID-19 pathology. Life Sci

581 Alliance [Internet]. 2022 Jan;5(1). Available from:
582 http://dx.doi.org/10.26508/lsa.202101168

583 53. Torretta E, Garziano M, Poliseno M, Capitanio D, Biasin M, Santantonio TA, et al.
584 Severity of COVID-19 Patients Predicted by Serum Sphingolipids Signature. Int J
585 Mol Sci [Internet]. 2021 Sep 22;22(19). Available from:
586 http://dx.doi.org/10.3390/ijms221910198

587 54. Fritsch SD, Weichhart T. Effects of Interferons and Viruses on Metabolism. Front
588 Immunol. 2016 Dec 21;7:630.

589

590 **Figures:**

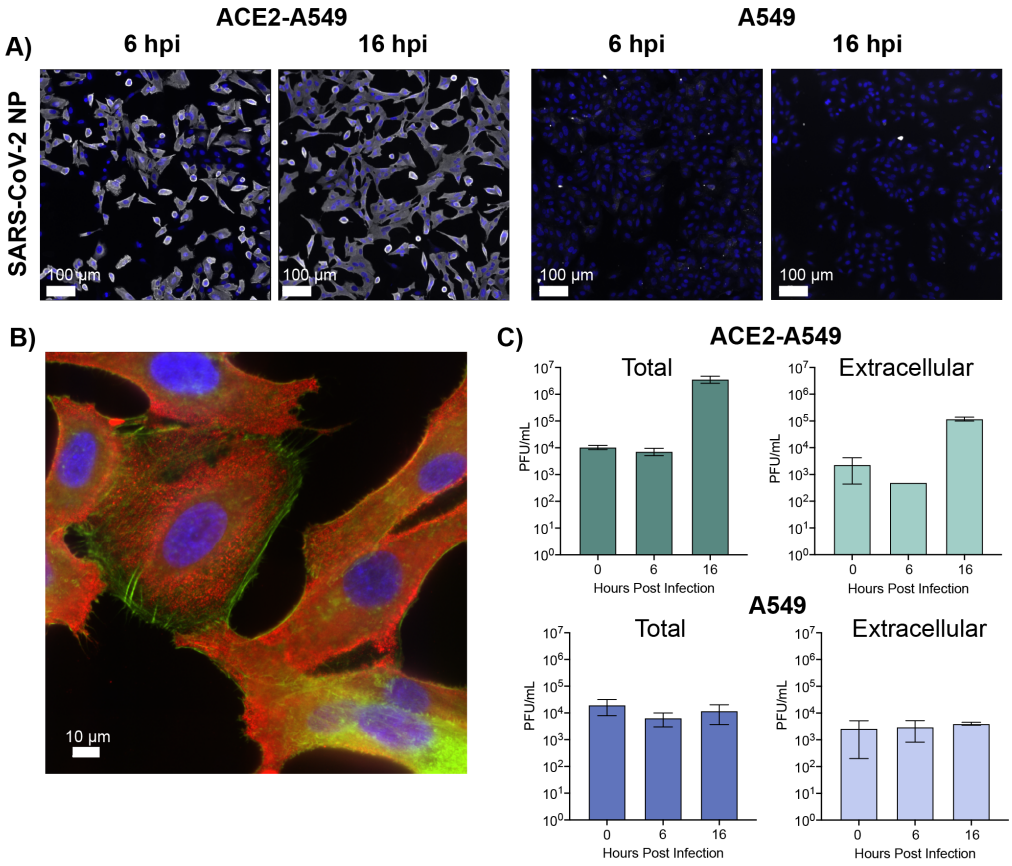

591

592 **Figure 1: Infection of different A549 cells with SARS-CoV-2. (A)** ACE-2 expressing
593 or parental A549 cells were infected at MOI 10 with SARS-CoV-2/WA01. Parallel
594 infections were fixed at 6 and 16 hpi and stained with SARS-CoV-2 anti-nucleocapsid
595 antibody (red) with Dapi (blue, nuclei). Scale bar is 100 µm. **(B)** Co-staining of the
596 SARS-CoV-2 anti nucleocapsid antibody (red) with phalloidin (green) with Dapi (blue,
597 nuclei) in Ace2-A549 cells at 16 hpi at MOI of 10. **(C)** Titers from Ace2-A549 and A549
598 cells infected with SARS-CoV-2 at an MOI 10. Both cell extracts (Total) and
599 supernatants (Extracellular) were collected and titered at 0, 6, and 16 hpi. All data
600 represented as the mean ± SD of three independent measurements.

601

602

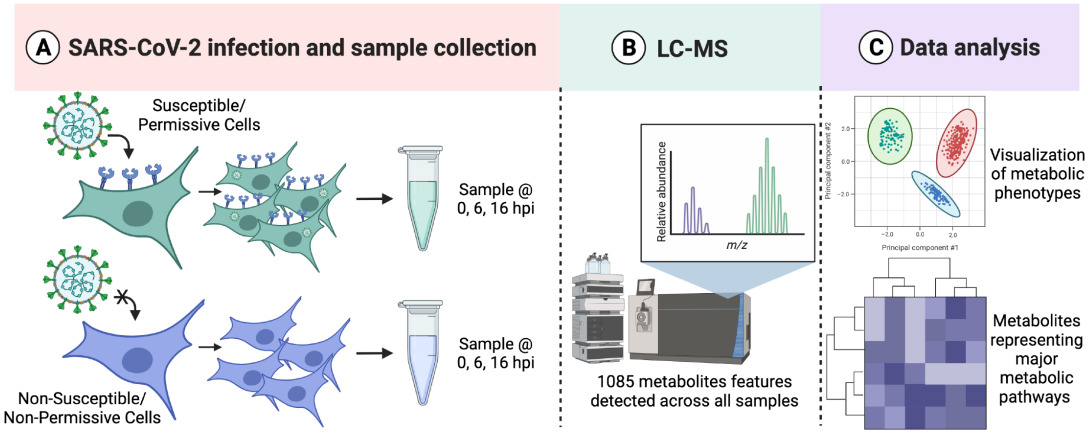

Figure 2. Metabolic profiling analysis pipeline for infected cells. (A) Ace2-A549 and A549 cells were infected with SARS-CoV-2 Isolate USA-WA1/2020 at an MOI of 10. Metabolites were extracted at multiple time points post infection. **(B)** Metabolic profiles are generated following LC-MS detection in the Mass Spectrometry Core Facility. **(C)** Data processing and analysis allows for both global metabolite profiling and pathway enrichment analysis. Image generated with Biorender.

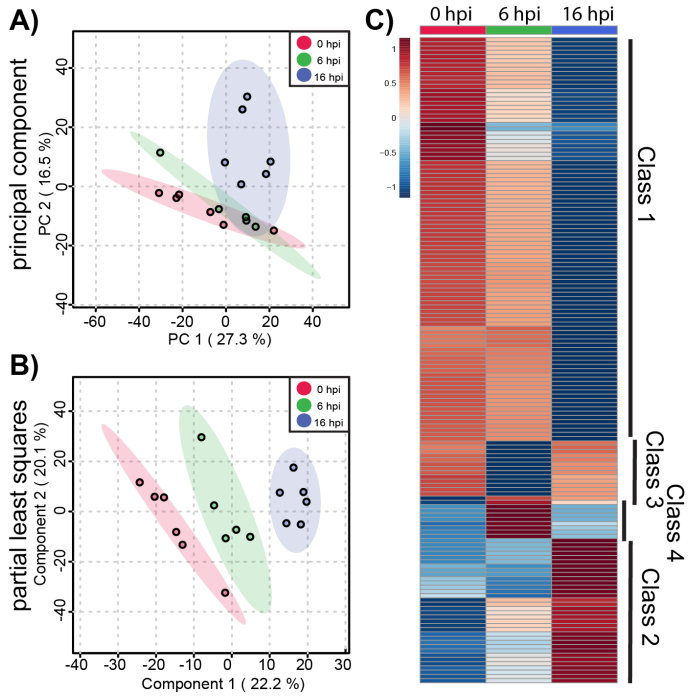

Figure 3. Global metabolite profiling of SARS-CoV-2 infected ACE2-A549 cells. A total of 1085 metabolites were analyzed by **(A)** principal component analysis (PCA) and **(B)** supervised partial least-squares discriminant analysis (PLSDA). **(C)** Heatmap analysis of significant metabolites (n=152) reveals temporal changes in metabolite phenotypes from 0 to 16 hpi. Mean intensities of each metabolite were clustered into 3 groups: 0 hpi (n=6), 6 hpi (n=5), and 16 hpi (n=6). Normalized fold change of specific metabolites is relative to peak concentration across 0, 6, and 16 hpi.

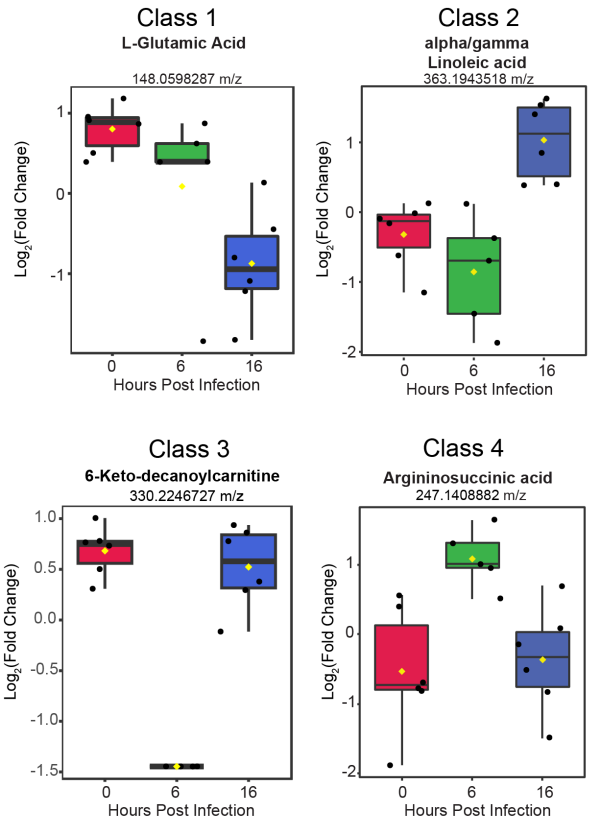

Figure 4. Putative metabolites identified from each of the four classes. The normalized fold change value for 4 separate metabolites are presented within box plots. Individual replicates within each time point are represented as black spots. Average value is the yellow diamond. Each plot is labeled for the individual metabolite(s) based on m/z value identification.

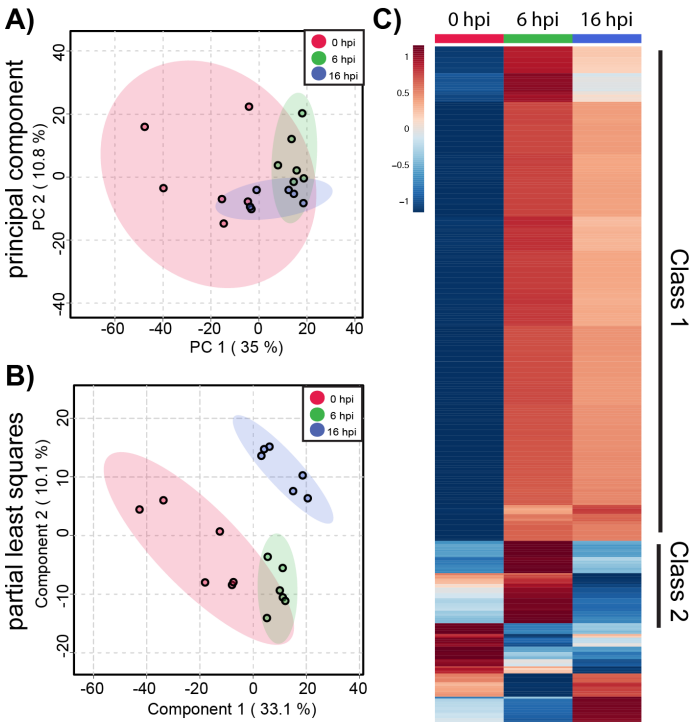

Figure 5. Global metabolite profiling of SARS-CoV-2 inoculated A549 cells. Similar to Ace2-A549 cells, metabolite profiles from A549 cells were compared by **(A)** PCA and **(B)** PLSDA. **(C)** Heatmap analysis of significant metabolites (n=377) reveals a different temporal phenotype in cells that are exposed to SARS-CoV-2 but remain uninfected. Mean intensities of each metabolite were clustered into 3 groups: 0 hpi (n=6), 6 hpi (n=6), and 16 hpi (n=6). Normalized fold change of specific metabolites is relative to peak concentration across 0, 6, and 16 hpi.

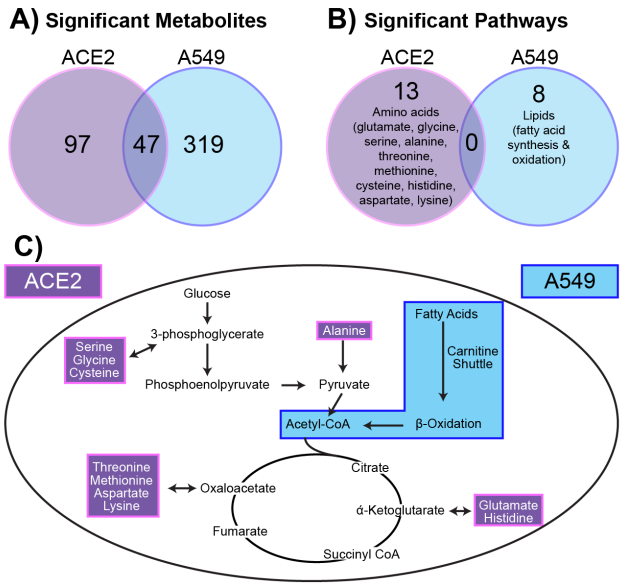

Figure 6: A549 cells have quantifiably different metabolic responses to SARS-CoV-2. (A) Significant metabolites (FC >1.5) from ACE2-A549 and A549 cells were compared to identify similar and different metabolites that change in response to SARS-CoV-2. **(B)** Pathway analysis on significant metabolites from ACE2-A549 and A549 cells. **(C)** Evaluating metabolic pathway changes relative to energy generation. Amino acids that were downregulated in Ace2-A549 are shown within the pathway highlighted in purple. Fatty acid metabolism was upregulated in A549 cells exposed to SARS-CoV-2, highlighted separately in blue. Both pathways directly or indirectly connect with components of the TCA cycle and glycolysis.

652 **Table 1:**

ACE2-A549 Pathways	Pathway total	Hits Total	Hits Sig	Gamma Value	Cpd.Hits
Glutamate metabolism	15	5	5	0.00558	L-Glutamic acid | Oxoglutaric acid | Gamma-Aminobutyric acid | Glutathione | Succinic acid semialdehyde
Glutathione Metabolism	19	4	4	0.009278	Pyroglutamic acid | L-Glutamic acid | Glutathione | L-Cysteine
Tryptophan metabolism	94	9	7	0.009861	L-Glutamic acid | Oxoglutaric acid | Formyl-5-hydroxykynurenamine | 2-Aminobenzoic acid | CE2095 | L-Kynurenine | Glutathione
Glycine, serine, alanine and threonine metabolism	88	8	6	0.015295	L-Glutamic acid | Oxoglutaric acid | Dimethylglycine | Creatine | 2-Ketobutyric acid | L-Allothreonine | L-Threonine | Glutathione
Methionine and cysteine metabolism	94	8	6	0.015295	L-Glutamic acid | Oxoglutaric acid | 2-Ketobutyric acid | DL-Glutamate | L-Cysteine | Allocystathionine | L-Cystathionine | Glutathione
Urea cycle/amino group metabolism	85	10	7	0.018261	L-Glutamic acid | Creatinine | Creatine | Argininosuccinic acid | Gamma-Aminobutyric acid | Oxoglutaric acid | Queuine | N4-Acetylaminobutanal
Histidine metabolism	33	3	3	0.01834	L-Glutamic acid | Oxoglutaric acid | Glutathione
Beta-Alanine metabolism	20	3	3	0.01834	L-Glutamic acid | Gamma-Aminobutyric acid | Oxoglutaric acid
Alanine and Aspartate Metabolism	30	4	3	0.041655	L-Glutamic acid | Oxoglutaric acid | N-Acetyl-L-aspartic acid | Argininosuccinic acid
Lysine metabolism	52	4	3	0.041655	L-Glutamic acid | Oxoglutaric acid | Pipecolic acid
Glycerophospholipid metabolism	156	6	4	0.042495	Alpha-Linolenic acid | Glycerophosphocholine | Phosphorylcholine | Linoleic acid
C5-Branched dibasic acid metabolism	10	2	2	0.045209	Itaconic acid | Mesaconic acid
Ascorbate (Vitamin C) and Aldarate Metabolism	29	2	2	0.045209	Glutathione | L-Erythrulose

653

654

655

656 **Table 2.**

A549 Pathways	Pathway total	Hits Total	Hits Sig	Gamma Value	Cpd.Hits
Di-unsaturated fatty acid beta-oxidation	26	5	5	0.00594	CE2422 | CE2421 | CE2434 | CE0849 | Linoleic acid
Fatty acid activation	74	9	6	0.011166	Palmitoyl-CoA | Alpha-Linolenoyl-CoA | Alpha-Linolenic acid | Gamma-Linolenic acid | Linoleic acid | Heptadecanoyl-CoA
Fatty Acid Metabolism	63	4	3	0.024423	3-Oxohexadecanoyl-CoA | Palmitoyl-CoA | Linoleic acid
Fatty acid oxidation	35	4	3	0.024423	Palmitoyl-CoA | Alpha-Linolenoyl-CoA | Heptadecanoyl-CoA
De novo fatty acid biosynthesis	106	7	4	0.031172	Palmitoyl-CoA | Alpha-Linolenic acid | Gamma-Linolenic acid | Linoleic acid
Leukotriene metabolism	92	7	4	0.031172	20-Hydroxy-leukotriene B4 | CE6473 | CE6228 | CE6182 | CE6187
Omega-3 fatty acid metabolism	39	2	2	0.034719	trans-2-Enoyl-OPC8-CoA | Alpha-Linolenic acid
Carnitine shuttle	72	5	3	0.040388	Alpha-Linolenoyl-CoA | Palmitoyl-CoA | Heptadecanoyl-CoA

657

658

659

660

Supplementary Figures

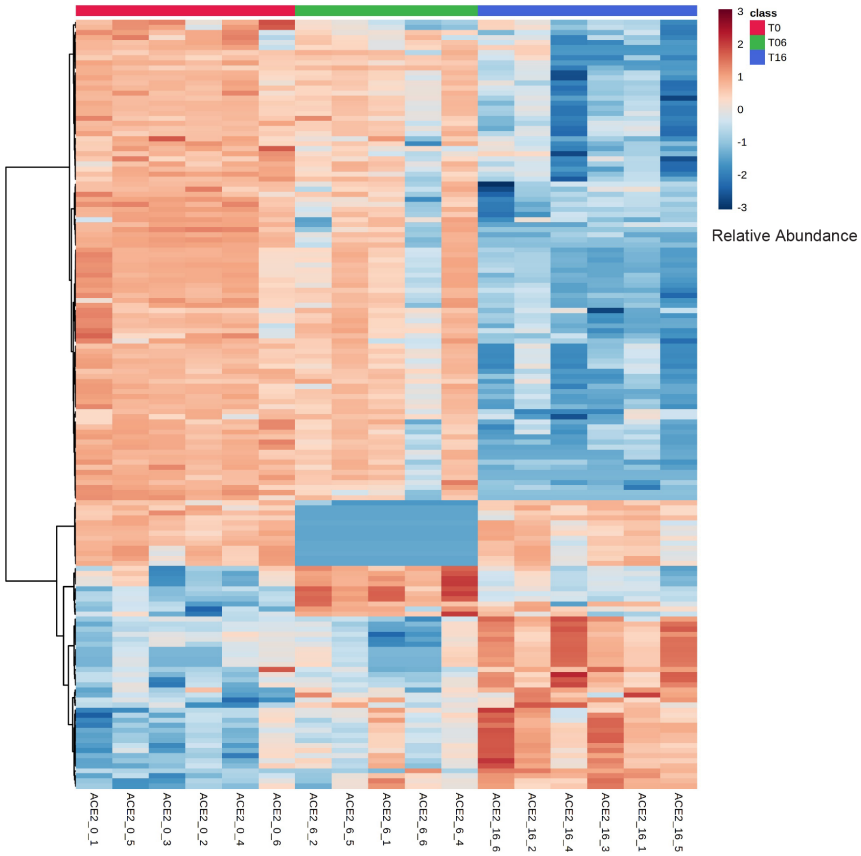

Figure S1: Heatmap analysis of significant metabolites (n = 152) for all ACE2-A549 samples at each time point.

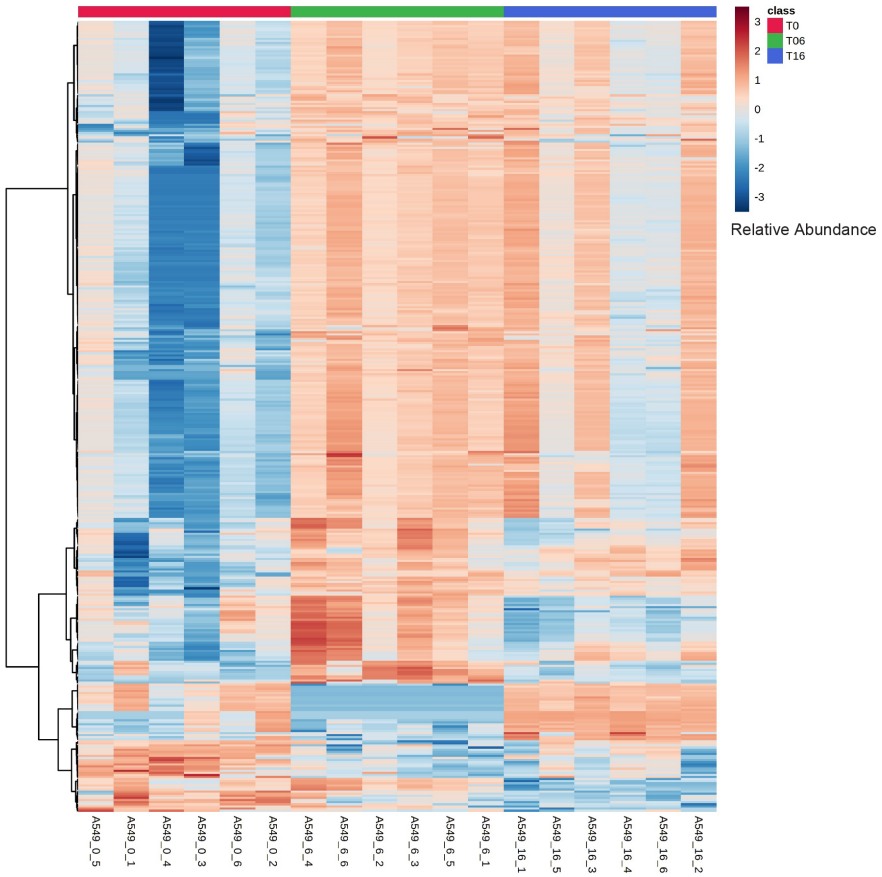

Figure S2: Heatmap analysis of significant metabolites (n = 377) for all A549 samples at each time point.

672 **Table S1:** Raw mass spec values for all samples and timepoints.